Quantum Electronics **50** (7) 662–666 (2020)

https://doi.org/10.1070/QEL17293

Three-colour digital holographic microscopy based on a Mach–Zender interferometer and a solid-state RGB laser

A.I. Lyashenko, O.V. Pol'shchikova, A.S. Machikhin, A.G. Vlasova, V.E. Pozhar, A.B. Kozlov

Abstract. **We have developed a facility for recording colour digital holograms involving a Mach–Zender interferometer and a pulsed solid-state RGB laser, which radiates simultaneously at three wavelengths: 451, 532, and 634 nm. These wavelengths are obtained in the conversion of the radiation of a pulsed Nd^{3+}:YAG laser (1064 nm), which operates in the regime of intracavity parametric oscillation at a wavelength of 1570 nm, with the subsequent conversion of its frequencies to the red, green, and blue spectral regions in nonlinear KTP-crystal elements. The combination of this three-wavelength pulsed light source with the Mach–Zender interferometer provides the simultaneous recording of three spectral digital holograms with one matrix RGB radiation detector. Pulsed three-colour digital holography shows promise for the analysis of fast processes and rapidly varying colour phase objects.**

Keywords: *three-colour digital holography, parametric oscillator, three-colour RGB laser.*

1. Introduction

Digital holographic microscopy (DHM) is based on the electronic recording of the interference pattern of objective and reference waves and is a modern technique employed widely to study biological and technical objects [1–3]. Using digital processing of interferograms it is possible to obtain accurate quantitative data both about the amplitude and the phase of the object wave reflected from the object under investigation or transmitted through it [4]. This permits determining the structure of the object and its properties not only in the transverse direction but also in the axial direction. In the reflection scheme, which is used in the study of opaque objects, the phase delay along the axis characterises the surface topography. In the transmission scheme, the phase delay is proportional to the optical path length of the light wave transmitted through the transparent object. The latter version is among the methods of quantitative phase microscopy, which is used to investigate so-called 'phase' objects. In this case, the axial resolution of DHM techniques may range up to the subnanometre level, while the axial resolution of a classical microscope amounts to a few micrometres [1].

Recent years have seen the development of three-colour DHM, characterised in that the recording of digital holograms and reconstruction of phase images are performed at three wavelengths in the red (R), green (G), and blue (B) regions of the spectrum. This permits extracting a more detailed information about the object: the thickness and refractive index of the sample [3], the spectral dependence of the phase delay and therefore of the refractive index. Furthermore, this permits obtaining multi-colour amplitude images [1] and improving the axial resolution [2].

There are several approaches to the solution of the problem of recording multi-colour digital holographic images [3, 5–14]. The methods in use require either mechanical displacement of components [1, 6, 7] (this imposes limitations on the measurement accuracy), or commutation or spectral realignment of the sources (in this case, the measurements are spaced in time), which limits the speed of the methods and hinders the operation with rapidly varying objects. Other factors also affect the sensitivity of the systems and their selectivity. The background illumination caused by the parasitic scattering from the system's elements is proportional to the spectral channel width, and so the use of broadband radiation entails a significantly lower contrast of the recorded interference pattern than the use of a narrowband one. This results in a growth of the uncertainty of phase reconstruction, and so it is expedient to design systems that provide highly selective simultaneous recording of several narrowband spectral holographic images and do not require mechanical spectral realignment.

In the present work we describe the three-colour DHM facility that makes use of the pulsed RGB laser made in the Scientific and Technological Centre of Unique Instrumentation of the Russian Academy of Sciences. The laser radiates simultaneously at wavelengths of 451, 532, and 634 nm, which cor-

A.I. Lyashenko, O.V. Pol'shchikova Scientific and Technological Centre of Unique Instrumentation, Russian Academy of Sciences, ul. Butlerova 15, 117342 Moscow, Russia;
A.S. Machikhin, A.G. Vlasova Scientific and Technological Centre of Unique Instrumentation, Russian Academy of Sciences, ul. Butlerova 15, 117342 Moscow, Russia; National Research University MEI, Krasnokazarmennaya ul. 14, 111250 Moscow, Russia;
V.E. Pozhar Scientific and Technological Centre of Unique Instrumentation, Russian Academy of Sciences, ul. Butlerova 15, 117342 Moscow, Russia; Bauman Moscow State Technical University (National Research University), Vtoraya Baumanskaya ul. 5, stroenie 1, 105005 Moscow, Russia; e-mail: v_pozhar@rambler.ru;
A.B. Kozlov Scientific and Technological Centre of Unique Instrumentation, Russian Academy of Sciences, ul. Butlerova 15, 117342 Moscow, Russia; OJSC M.F. Stel'makh Polyus Research Institute, ul. Vvedenskogo 3, stroenie 1, 117342 Moscow, Russia

Received 18 February 2020; revision received 19 March 2020
Kvantovaya Elektronika **50** (7) 662–666 (2020)
Translated by E.N. Ragozin

respond to the quantum efficiency maxima of the matrix detectors of colour video cameras in the red, green, and blue spectral regions. The DHM systems based on this laser are free from the drawbacks described above.

2. Three-colour RGB laser

The three-colour RGB laser, which synchronously generated high-power single pulses with duration in the nanosecond range, was made on the basis of a pulsed Nd^{3+}:YAG laser, which operated in the regime of an electro-optically Q-switched cavity with an optical parametric oscillator (OPO) using a KTP ($KTiOPO_4$) crystal. The neodymium $\lambda_p = 1064$ nm laser radiation is most efficiently converted to the radiation at a wavelength $\lambda_s = 1570$ nm, which is eye-safe, in the intracavity parametric oscillation, when the OPO is accommodated inside the laser cavity [15–17]. The optical configuration of the RGB laser is schematised in Fig. 1.

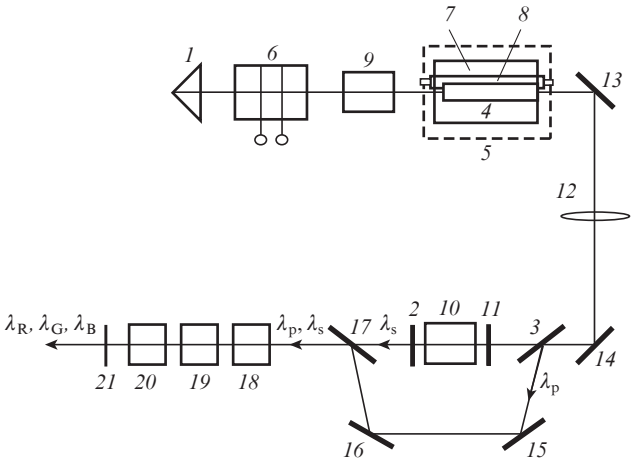

Figure 1. Optical configuration of the RGB laser (see the body of text for designations).

The cavity is made up of a roof prism (*1*) and an output mirror (*2*), which reflects the λ_p radiation completely and is partly transparent to the λ_s radiation. The λ_p radiation may also be extracted with a polariser plate (*3*). The cylindrical Nd^{3+}:YAG crystal active element (*4*) grown in the $\langle 100 \rangle$ direction is so oriented that the crystal axes Y and Z form angles of ±45° with the transmission plane of the polariser (*3*) (the plane of Fig. 1). The laser head (*5*) comprises a cylindrical specular reflector (*7*), an active element (*4*), and a pumping flashlamp (*8*). Placed between the DKDP (KD_2PO_4) crystal electro-optical (EO) element (*6*) and the active element (*4*) is a 90° polarisation plane rotator (*9*) made of optically active crystalline quartz, which provides partial mutual cancellation of the birefringence induced in the active and EO elements. The use of the roof prism (*1*) in the optical configuration provides a more uniform cross-sectional gain distribution for the specified 45° orientation of the active element relative to the horizontal plane [16]. The cavity of the OPO, which is based on the nonlinear element (*10*) of an x-cut KTP crystal, is formed by a mirror (*2*) and a parametric mirror (*11*), which is highly reflecting for the λ_s radiation and is optimised for maximum transmittance for the λ_p radiation. A positive lens (*12*) and two mirrors (*13*) and (*14*) are located between the active element (*4*) and the polariser (*3*). Positioning the EO element (*6*) and polariser (*3*) in the cavity on different sides of the active element (*4*) made it possible to realise three different operating modes in this device: a laser with an 'EO mirror' (λ_p), an 'eye-safe' laser (λ_s), and a two-frequency laser (λ_p and λ_s).

The laser with the 'EO mirror' was Q-switched by changing its reflection coefficient. During the accumulation of population inversion in the active element (*4*), the 'EO mirror', which is formed by the roof prism (*1*), EO element (*6*), and polariser (*3*), has a low reflection coefficient R_{eo}, which is provided by the initial alignment of the Z axis of the element (*6*) at small (2– 3°) angles relative to the cavity axis {see Ref. [16], formulas (1) and (2)}. In this case, the initial value of the R_{eo} coefficient ensures the fulfilment of the condition:

$$K_{max} = K_{th}, \tag{1}$$

where K_{max} is the peak gain of the active element during the pump pulse and K_{th} is the threshold gain due to losses in the cavity. On reaching the maximum gain K_{max} (in a time $\Delta t_{opt} \approx 20$ μs), the 'EO mirror' characteristics approach the optimal value, which results in the formation of single radiation pulse λ_p extracted from the cavity via the polariser (*3*). The OPO cavity characteristics are so selected that the power of this pulse is sufficiently high to generate a radiation pulse λ_s. The laser performance characteristics are provided by placing the lens (*12*) to concentrate the λ_p radiation in the OPO cavity, employing the nonlinear optical element (*10*) of sufficient length (4 × 4 × 16 mm), and selecting the optimal reflection coefficient of the mirror (*2*) at the wavelength λ_s.

The reflection coefficient R_{eo} in the laser with the 'EO mirror' is optimised by applying a high-voltage pulse with an amplitude $U_{opt} \approx 2$ kV to the electrodes of the EO element. This permits maximising the energy of λ_p radiation single pulses delivered to the output stage of the RGB laser in the reflection from the polariser (*3*).

The generation of radiation at the signal wavelength λ_s sets in when a voltage pulse with an amplitude $U \approx 5$ kV is applied to the electrodes of the element (*6*), with the pulse energies peaking at

$$U_0 = (4n_o d/\lambda_p)(n_o^2/n_e^2 - 1)\psi\theta U_{\lambda/4}, \tag{2}$$

where n_o and n_e are the refractive indices of the ordinary and extraordinary waves, respectively; d is the EO element length; ψ and θ are the angles which its Z axis forms with the cavity axis; and $U_{\lambda/4}$ is its quarter-wave voltage [16].

When a voltage pulse of intermediate amplitude U ($U_{opt} < U < U_0$) is applied to the electrodes of the element (*6*), the two-frequency laser springs into operation, with the λ_p radiation reflecting from the polariser (*3*) and the λ_s radiation emanating from the mirror (*2*). The λ_s and λ_p output laser beams are brought together using a set of mirrors (*15*) and (*16*) and a polariser (*17*) (see Fig. 1). The energies of the pulses at these wavelengths are increased by increasing the energy of pump flashlamp pulses. In this case, the laser switches to the Q-switching regime after the cessation of free-running oscillation [18]. When the above conditions are fulfilled [threshold (1) is achieved, the instant of Q-switching is delayed by a time Δt_{opt}, and the OPO is excited by application of voltage $U \approx U_0$], the probability of damage of the

dielectric mirrors and the end faces of the nonlinear element of the OPO as well as of other optical elements of the cavity becomes negligible.

In the output stage of the RGB laser, in the nonlinear optical element (*18*) (KTP, $\theta = 53°$, $\varphi = 0°$) there occurs generation of the sum-frequency radiation, $1/\lambda_R = 1/\lambda_p + 1/\lambda_s$, which lies in the red part of the spectrum ($\lambda_R = 634$ nm). In the next element (*19*) (KTP, $\theta = 70°$, $\varphi = 30°$) there occurs generation of another sum frequency $1/\lambda_B = 1/\lambda_s + 1/\lambda_R$, which belongs to the blue part of the spectrum ($\lambda_B = 451$ nm). The residual radiation with the wavelength λ_p is converted to the green second-harmonic radiation ($\lambda_G = 532$ nm) in the element (*20*) (KTP, $\theta = 90°$, $\varphi = 23°$) [17]. By gradually adjusting the voltage U in the above range, it is possible to achieve a uniform mixing of the three colours to obtain a total of white light. Placed at the output of the RGB laser is a mirror (*21*), which cuts off the IR radiation.

The results of independent Nd^{3+}:YAG laser tests with the DKDP EO element and the KTP nonlinear element bear out the efficiency of the developed scheme. For a pump pulse energy of 10 J, the highest energies of the radiation pulses with $\lambda_p = 1064$ nm and $\lambda_s = 1570$ nm are 80 and 30 mJ, respectively, for a pulse repetition rate of up to 100 Hz. In this case, the respective energies of the 634, 451, and 535 nm pulses are 5, 2, and 7 mJ.

In the experiments of the present work we employed an RGB laser with a significantly lower power, which operated at a pulse repetition rate of 20 Hz. Its main characteristics and radiation monopulse parameters are collected in Table 1.

Table 1. Characteristics and parameters of RGB laser single pulses.

Channel	Centre wavelength/ nm	Spectral width/ nm	Pulse duration/ ns	Average power/ mW	Pulse energy/ mJ
R	634	0.08	4	0.6	0.024
G	532	0.03	10	0.9	0.036
B	451	0.02	8	0.2	0.008

3. Facility for three-colour digital holographic microscopy

To demonstrate the efficiency of using the newly developed RGB laser in three-colour DHM, we assembled a facility based on the classical Mach–Zender interferometer (Fig. 2) and The Imaging Source DFM 42BUC03-ML colour camera with a global-shutter 1280 × 960 array sensor with 3.75 × 3.75-μm pixels.

The RGB-laser radiation is directed to the interferometer input and is split with a beam splitter BS1 into beams: the object beam and the reference one. The former illuminates the object O under investigation via condenser lens L1. The object is imaged on the radiation detector RD with a microlens ML and the system of lenses L2–L4. When passing through the object the wave acquires a phase delay $\Delta\varphi \approx 2\pi nL/\lambda$ proportional to the thickness L and the refractive index n of the sample. Located in the reference arm is the system of mirrors M3–M6, which permits compensating for the path difference between the interferometer arms. The beam splitter BS2 brings together the reference and object beams at a small angle, which next pass through an additional magnifying system comprising lenses L3 and L4 to interfere in the plane of the video camera sensor. For the optimal (according to

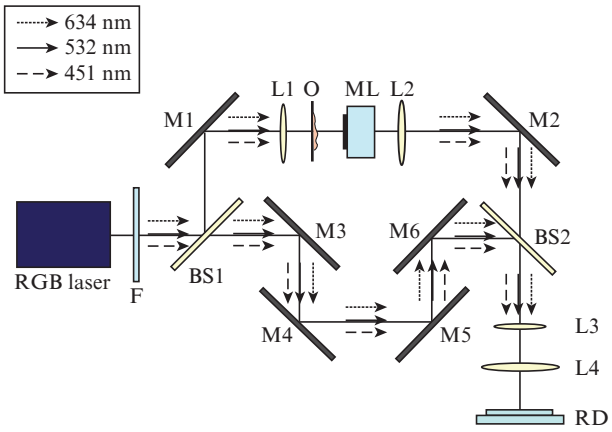

a

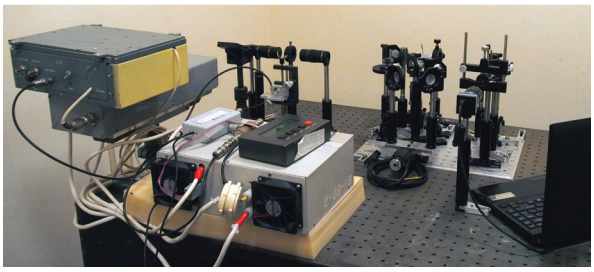

b

Figure 2. (a) Schematic and (b) external appearance of the facility intended for three-colour digital holography with the use of the RGB laser:
(F) neutral density filter; (BS1, BS2) beam splitters; (M1–M6) plane mirrors; (L1–L4) lenses; (O) object under investigation; (ML) microlens; (RD) radiation detector.

Kotel'nikov theorem) recording of the interference pattern, the angle between the beams at the input of the magnifying system should not exceed 1.8°.

Since the green component of the RGB laser is brighter than the red and blue ones, it was attenuated with the use of a set of band filters. The three-colour DHM facility reliant on the RGB laser permits recording three spectral holograms simultaneously with the use of an ordinary three-colour RGB radiation detector. This approach permits three-colour data to be obtained in one radiation pulse for a relatively simple alignment procedure and a high reliability.

4. Experimental results

The simultaneous recording of holograms using the radiation detector with a Bayer colour filter array makes it possible to obtain interference images at three wavelengths. However, the overlap of the sensitivity spectra of three colour (R, G, B) array filters gives rise to cross-spectral interference, since the hologram formed by one of the monochromatic components of the source generates response in all three detection channels. To correct the recorded spectral holograms, use should be made of the sensitivity matrix $K_{\alpha\beta}$ [19]. The further digital processing of the holograms comprises the following stages: filtering and centring of the –1st order Fourier transform of a hologram; inverse Fourier transform; calculation of the phase delay distribution; application of a phase unwrapping (stitching) procedure to each pixel of the phase image [8]. Eventually obtained is the spectral dependence of the spatial phase delay introduced by the object under investigation.

The newly developed facility was used to obtain the phase maps of different objects. Figure 3 depicts the data of the experiment in which the test object was a Fresnel lens etched in an SU-8 photoresist layer. Shown in the drawing are the recorded colour interference pattern of the object, its decomposition into three spectral channels, and the corresponding calculated phase maps.

To test the facility, the characteristics of this Fresnel lens were measured with an atomic-force microscope and a white-light interferometer (Fig. 4). The lens groove depth h was

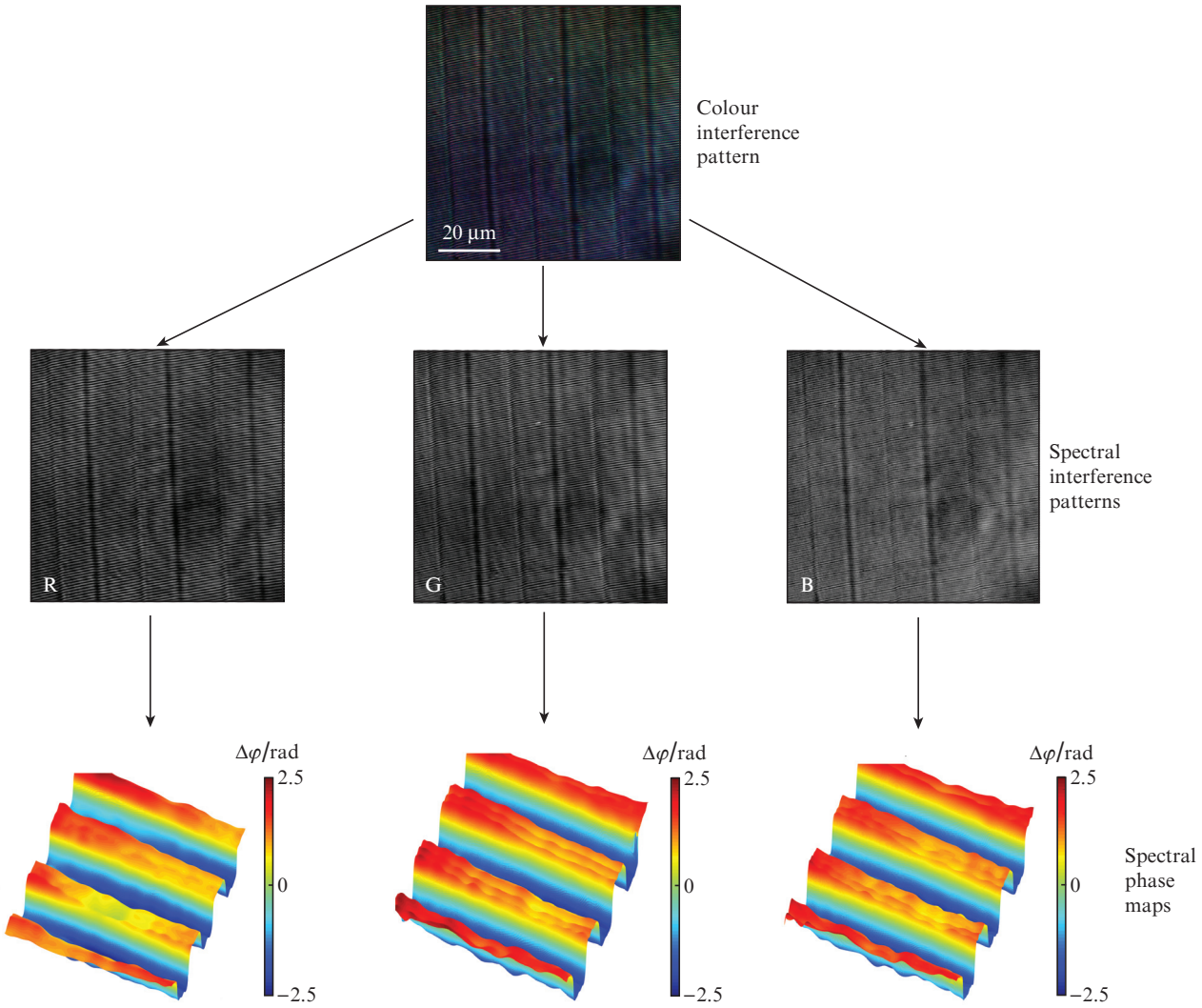

Figure 3. (Colour online) Measurement of Fresnel lens topography with three-colour DHM.

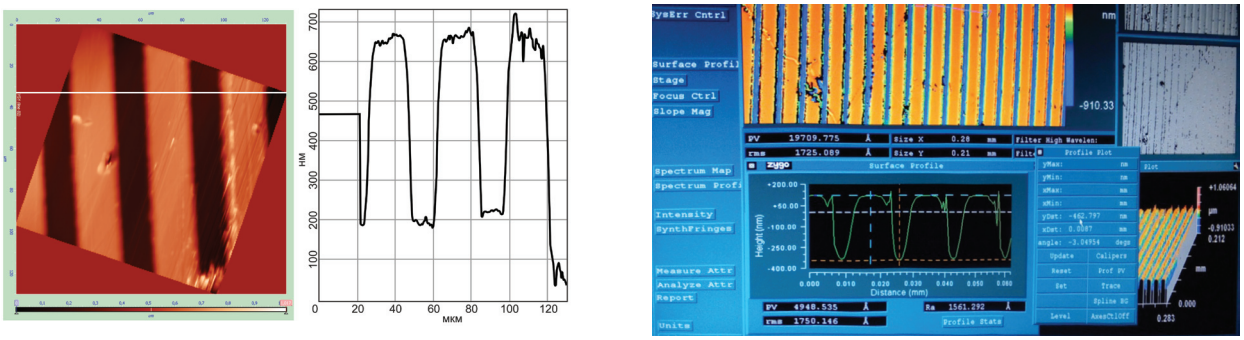

a b

Figure 4. Measurement of Fresnel lens topography (a) with an atomic-force microscope and (b) a white-light interferometer.

measured at 455 and 463 nm, respectively, which is close to the depth values obtained using the three-colour DHM: h_R = 474 nm, h_G = 485 nm, and h_B = 463 nm, which testifies to the correctness of the measurements performed.

5. Conclusions

The RGB laser developed on the basis of a pulsed Nd^{3+}:YAG laser permits adjusting the intensity ratio of the three colour radiation components. The three-colour lasing regime is implemented due to the intracavity optical parametric oscillator with a KTP crystal as well as three external nonlinear optical KTP-crystal elements, which produce the sum and second harmonic frequencies in the red (634 nm), green (532 nm) and blue (451 nm) spectral domains.

The three-colour DHM scheme developed on the basis of this laser provides an instantaneous (limited by photodetector speed) and reproducible recording of three colour digital holograms at wavelengths corresponding to the sensitivity peaks of conventional colour video cameras. This permits the two-dimensional phase delay distribution, as well as the map of refractive index or object thickness, to be determined at three wavelengths without spectral readjustment. The outlined three-colour DHM facility may therefore be validly employed in the prompt analysis of the structural elements of the objects under investigation, including the rapidly varying ones.

Acknowledgements. This work was performed with the use of equipment of the Centre for Shared Research Facilities at the Scientific and Technological Centre of Unique Instrumentation, Russian Academy of Sciences.

References

1. Yamaguchi I., Matsumura T., Kato J. *Opt. Lett*., **27**, 1108 (2002).
2. Fu Y., Pedrini G., Hennelly B.M., Groves R.M., Osten W. *Opt. Lasers Eng*., **47**, 552 (2009).
3. Park Y., Yamauchi T., Choi W., Dasari R., Feld M.S. *Opt. Lett*., **34**, 3668 (2009).
4. Vishnyakov G.N., Levin G.G., Minaev V.L. *Izmeritel'naya Tekhnika*, **11**, 34 (2015).
5. Fu D., Choi W., Sung Y., Yaqoob Z., Dasari R.R., Feld M. *Biomed. Opt. Express*, **1**, 347 (2010).
6. Dubey V., Singh G., Singh V., Ahmad A., Mehta D.S. *Appl. Opt*., **55**, 2521 (2016).
7. Kalenkov S.G., Kalenkov G.S., Shtanko A.E. *J. Opt. Soc. Am. B*, **4**, B49 (2017).
8. Machikhin A., Polschikova O., Ramazanova A., Pozhar V. *J. Opt*., **19**, 075301 (2017).
9. Popescu G., Bhaduri B., Pham H. Patent US 8837045 B2, 16.09.2014.
10. Pham H., Bhaduri B., Ding H., Popescu G. *Opt. Lett*., **37**, 3438 (2012).
11. Mann C.J., Bingham P.R., Paquit V.C., Tobin K.W. *Opt. Express*, **16**, 9753 (2008).
12. Desse J.M., Picart P., Tankam P. *Meas. Sci. Technol*., **22**, 064005 (2011).
13. Toge H., Fujiwara H., Sato K. *Proc. SPIE*, **6912**, 69120U (2008).
14. Desse J.-M., Picart P., Tankam P. *Opt. Express*, **16**, 5471 (2008).
15. Dmitriev V.G., Tarasov L.V. *Prikladnaya nelineinaya optika* (Applied Nonlinear Optics) (Moscow: Fizmatlit, 2004).
16. Lyashenko A.I., Pavlovich V.L. Patent RU 2101817 C1, 10.01.1998.
17. Alampiev M.V., Lyashenko A.I., in *Trudy Ross. Nauchno-Tekhnich. Obshchestva Radiotekhniki, Elektroniki i Svyazi im. A.S. Popova. Ser. Akustoopticheskie i Radiolokatsionnye Metody Izmerenii i Obrabotki Informatsii.* (Proc. of the Russian Scientific and Technical A.S. Popov Society for Radio Engineering, Electronics, and Communications. Ser. Acoustooptical and Radar Methods of Measurements and Information Processing) Issue X (Moscow, Suzdal', 2017) p. 184.
18. Alampiev M.V., Lyashenko A.I., Shvom E.M. Patent RU 2176839 C1, 12.01.2001.
19. Machikhin A.S., Poschikova O.V., Vlasova A.G., Lyashenko A.I., Dmitriev I.V., Batshev V.I., Bulatov M.F., Pozhar V.E. *Opt. Lett*., **44**, 5025 (2019).